

# Electron and atomic force microscopy of the trimeric ammonium transporter AmtB

Matthew J. Conroy<sup>1</sup>, Stuart J. Jamieson<sup>1†</sup>, Daniel Blakey<sup>2‡</sup>, Thomas Kaufmann<sup>3</sup>, Andreas Engel<sup>3</sup>, Dimitrios Fotiadis<sup>3</sup>, Mike Merrick<sup>2</sup> & Per A. Bullough<sup>1+</sup>

<sup>1</sup>Department of Molecular Biology and Biotechnology, Krebs Institute for Biomolecular Research, University of Sheffield, Sheffield, UK, <sup>2</sup>Department of Molecular Microbiology, John Innes Centre, Norwich, UK, and <sup>3</sup>ME Müller Institute for Structural Biology, Biozentrum, University of Basel, Basel, Switzerland

***Escherichia coli* AmtB is an archetypal member of the ammonium transporter (Amt) family, a family of proteins that are conserved in all domains of life. Reconstitution of AmtB in the presence of lipids produced large, ordered two-dimensional crystals. From these, a 12 Å resolution projection map was determined by cryoelectron microscopy, and high-resolution topographs were acquired using atomic force microscopy. Both techniques showed the trimeric structure of AmtB in which each monomer seems to have a pseudo-two-fold symmetry. This arrangement is likely to represent the *in vivo* structure. This work provides the first views of the structure of any member of the Amt family.**

Keywords: atomic force microscopy; electron microscopy; membrane protein; ammonium transport; projection structure

EMBO reports (2004) 5, 1153–1158. doi:10.1038/sj.embor.7400296

## INTRODUCTION

The transport of ammonium across the cell membrane is important in nearly all organisms, although the mechanism is not fully understood. It is known, however, that high-affinity ammonium transporters (Amt) constitute a distinct protein family found in all domains of life (von Wirén & Merrick, 2004). Many organisms encode several Amt paralogues that show different affinities for

ammonium (or methylammonium), and in higher eukaryotes, these paralogues are expressed in a tissue-specific fashion (von Wirén *et al*, 2000).

In animals, the Amt proteins are represented by the Rhesus (Rh) proteins (Marini *et al*, 2000). In humans, some Rh paralogues are expressed in the erythrocyte membrane (Eyers *et al*, 1994) and others are expressed in the kidney, liver and skin, the main organs of ammonia genesis (Quentin *et al*, 2003). Evidence is accumulating that the Rh proteins facilitate the transport of ammonium (Westhoff *et al*, 2002).

*Escherichia coli* contains a single Amt gene (*amtB*), which encodes a 428-amino-acid polypeptide (AmtB) with a deduced molecular mass of 44.5 kDa. The protein was predicted to have 12 transmembrane  $\alpha$ -helices (TMH) with both termini located in the cytoplasm (Thomas *et al*, 2000). However, recent work indicates that the first predicted TMH is actually a signal sequence, which is cleaved to leave a mature, 11 TMH protein of 406 residues with a periplasmic N-terminus (von Wirén & Merrick, 2004). This 11 TMH structure is characteristic of Amt proteins from bacteria, fungi and plants but not of Rh proteins, which have 12 TMH (Eyers *et al*, 1994).

*E. coli* AmtB purifies in detergent solution as a homotrimeric complex with a molecular mass of 135 kDa (Blakey *et al*, 2002). So far, *E. coli* AmtB is the only Amt protein to have been purified, but genetic and biochemical evidence indicates that Amt proteins from fungi and higher plants also form oligomeric complexes (Marini & Andre, 2000; Monahan *et al*, 2002; Ludewig *et al*, 2003). The erythroid Rh proteins have been proposed to form hetero-oligomers (Eyers *et al*, 1994).

Despite their important role in cellular metabolism, there have been no structural studies on Amt proteins. In this paper, we report the first structural view of a member of this protein family. We describe the reconstitution of *E. coli* AmtB into two-dimensional (2D) crystals and their imaging by cryoelectron microscopy (cryoEM) and atomic force microscopy (AFM), both of which show the likely *in vivo* structure when viewed perpendicular to the membrane.

<sup>1</sup>Department of Molecular Biology and Biotechnology, Krebs Institute for Biomolecular Research, University of Sheffield, Firth Court, Western Bank, Sheffield S10 2TN, UK

<sup>2</sup>Department of Molecular Microbiology, John Innes Centre, Colney Lane, Norwich NR4 7UH, UK

<sup>3</sup>ME Müller Institute for Structural Biology, Biozentrum, University of Basel, Klingelbergstrasse 50/70, 4056 Basel, Switzerland

<sup>†</sup>Present address: Avecia Biotechnology, Belasis Avenue, Billingham, Cleveland TS23 1YN, UK

<sup>‡</sup>Present address: Department of Human Anatomy and Genetics, University of Oxford, South Parks Road, Oxford OX1 3QX, UK

<sup>+</sup>Corresponding author. Tel: +44 114 2224245; Fax: +44 114 2222800; E-mail: p.bullough@shef.ac.uk

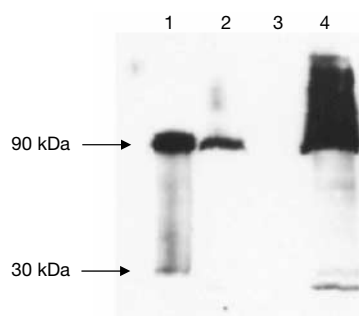


**Fig 1** | Western blot of protein extracts from wild-type *E. coli* strain ET8000 grown under nitrogen limitation to induce expression of AmtB from its native promoter. Lane 1 is from a His-tagged construct, while all other lanes are wild type. Lane 1: purified AmtB; lane 2: whole-cell extract; lane 3: cytoplasmic fraction; lane 4: membrane fraction. Samples were separated on a 10% SDS–polyacrylamide gel and visualized with a rabbit polyclonal anti-AmtB antibody.

## RESULTS

### AmtB is trimeric in the native cell membrane

Polyclonal antibodies prepared against purified AmtB were used in a western blot of cellular fractions from wild-type *E. coli* grown under nitrogen limitation. This blot identified a principal band with an apparent molecular mass of ~90 kDa and a mobility identical to that of purified trimeric AmtB. A minor fraction (<5%) was observed as a monomeric species of about 30 kDa. AmtB is completely localized in the membrane fraction (Fig 1). These data confirm that *E. coli* AmtB is almost exclusively trimeric when expressed at normal levels from the native *amtB* promoter, and that it is extremely stable in the presence of SDS.

### Crystallization and AFM

The best-ordered 2D crystals were formed from a mixture of AmtB and 1,2-dimyristoyl-*sn*-glycero-3-phosphatidylcholine (DMPC) at a lipid:protein ratio (LPR) of 1.0 (w/w). Crystals formed as (>3 μm on an edge) angular edged sheets. AFM of AmtB crystals showed that the majority are 127±3 Å thick (labelled ‘3’ in Fig 2), sufficient to accommodate two bilayers stacked together, although 63±2 Å ‘single’ thicknesses (labelled ‘2’ in Fig 2) could sometimes be seen at the margins of these sheets. Adjacent particles were of the same height, suggesting that all molecules in the crystal have the same orientation relative to the membrane plane. While the 127-Å-thick layers showed much greater crystalline order than the 63 Å layers, it is apparent from Fig 2B that particles in both types of layer show the same surface characteristics, implying that both ‘single’ and ‘double’ layers show the same surface of the protein to the AFM tip. Thus, double-layered crystals are most likely to be composed of two membranes stacked ‘head-to-tail’. At a higher magnification, AFM topographs (Fig 3) showed ordered arrays of particles each of which showed three prominent protrusions (arrows) 15 Å from the three-fold symmetry centre and a further three more peripheral protrusions (arrowheads) 34 Å from the centre. Correlation averages of 213 trimers (Fig 3C,D) show these features clearly.

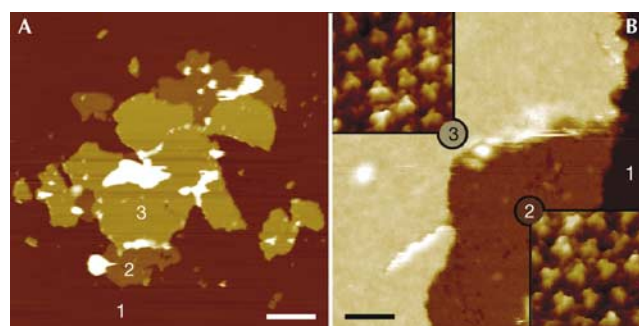


**Fig 2** | Morphology of crystals. (A) Overview AFM topograph of single- and double-layered AmtB sheets adsorbed on mica. Regions denoted with numbers 1, 2 and 3 correspond to double, single-layered sheets and double-layered sheets, respectively. (B) AFM image of a crystal recorded at the border between single- and double-layered sheets. The insets show scans of regions 2 and 3 at higher magnification. The topographs in the insets of (B) are shown in relief, tilted by 2°. Scale bars represent 2 μm (A) and 120 nm (B). Vertical brightness ranges: 25 nm (A) and 20 nm (B). Frame sizes are 32 nm for the insets in (B).

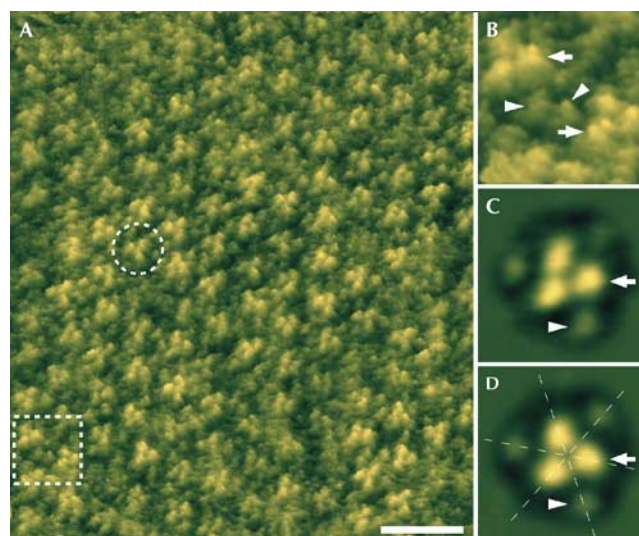


**Fig 3** | High-resolution AFM of AmtB. (A) Height image of the upper layer of a double-layered 2D crystal. An AmtB trimer is marked by the broken circle. The area indicated by the broken frame is magnified in (B). (C) Correlation average of 213 AmtB trimers and (D) with three-fold symmetrization. The arrows mark the prominent protrusions near the three-fold axis of the AmtB trimer and the arrowheads indicate the smaller, peripheral protrusions; the dashed lines indicate apparent pseudo-two-fold symmetry axes. The topographs in (A,B) are shown in relief, tilted by 15°. Scale bar in (A): 15 nm. Frame size in (B): 12.3 nm. Vertical brightness ranges: 1.3 nm (A,B) and 1.2 nm (C,D). Frame sizes in (C,D): 11.2 nm.

### Cryoelectron microscopy

CryoEM showed crystals with unit cell dimensions  $a = b = 157.5 \pm 1.5 \text{ \AA}$  and  $\gamma = 119 \pm 0.7^\circ$ . The Fourier components of one image are represented in supplementary Fig 1 online.

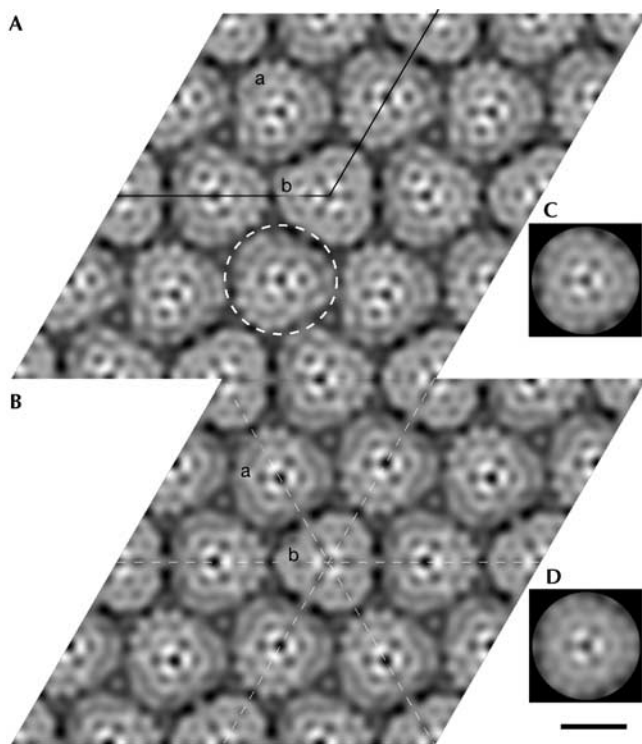


**Fig 4** | CryoEM projection maps of AmtB to 12 Å resolution, represented as grey levels. White corresponds to maximum density. (A) Map from six merged images of AmtB crystals with  $p3$  symmetry imposed. One unit cell is outlined. The dashed circle denotes one trimeric particle of AmtB. (B) Projection map as in (A), but with  $p321$  symmetry imposed. The unit cell is not outlined but is the same as in (A). The dashed lines show two-fold symmetry axes. In both maps, the two crystallographically independent particles are labelled 'a' and 'b'. (C,D) Three-fold rotationally averaged density maps of particle 'b' from the  $p3$  and  $p321$  maps, respectively. Scale bar, 50 Å.

Analysis of predicted symmetry-related phases to 12 Å resolution showed the data to be consistent with  $p3$  and  $p321$  symmetry (see supplementary data online). Amplitudes and phases from the six best images were averaged with  $p3$  or  $p321$  symmetry imposed, giving phase residuals to 12 Å resolution of 59.4° and 59.2°, respectively (see supplementary data online for a more detailed analysis). Projection maps are shown in Fig 4. Both maps show similar features; one unit cell (outlined in Fig 4A) contains four triangular particles, approximately 53 Å on a side. One particle, 'b', lies on a strict three-fold crystallographic symmetry axis. The three remaining (crystallographically equivalent) particles, 'a', do not lie on a crystallographic symmetry axis in the  $p3$  map, but are each bisected by an in-plane crystallographic two-fold axis in the  $p321$  map. In this instance, three such two-fold axes also bisect particle 'b'.

In both maps, those particles ('a') that do not lie on a crystallographic three-fold axis nevertheless seem to show three-fold symmetry, confirmed by determining rotational correlation coefficients for these particles. An unambiguous three-fold symmetry is shown for particles from both maps (Fig 5A). The

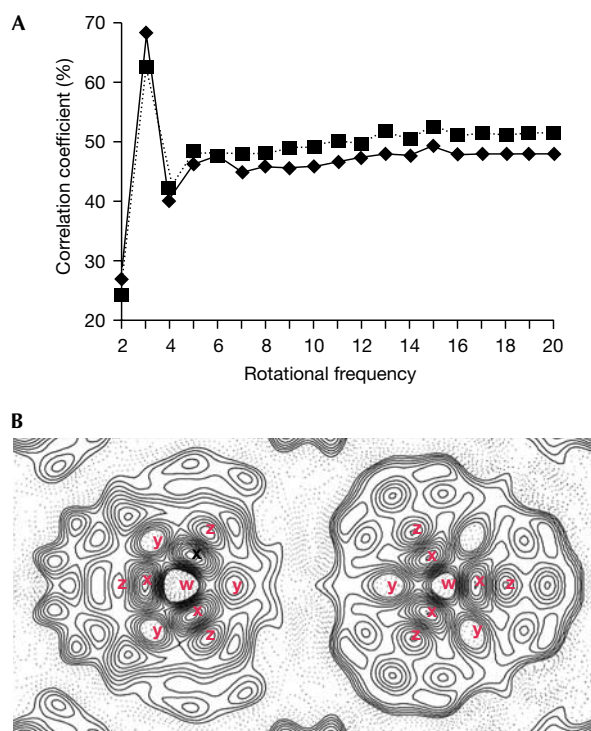


**Fig 5** | Features of the AmtB trimer. (A) Rotational correlation analysis of particles 'a' from  $p3$  (solid line) and  $p321$  (dotted line) maps that do not lie on a crystallographic three-fold axis. (B) Contour plot of particles from the  $p321$  map, one of which (right) lies on the crystallographic three-fold axis while the other (left) is bisected by a single two-fold axis only. Both particles show a low-density region (w), surrounded by three peaks of high density (x) and a ring of six areas of lower density (y and z); those marked with the same letter are related by either crystallographic (right) or noncrystallographic (left) three-fold symmetry.

similarity of the two crystallographically independent particles is even more apparent when three-fold averaging is applied to particle 'a' from either map (Fig 4C,D), and was confirmed by a rotational alignment of particle 'a' on 'b', giving maximum correlations of 98.7% and 98.4% for  $p3$  and  $p321$  maps, respectively.

The density features common to both particles are indicated in Fig 5B. Each particle contains a central region of low density, marked 'w', surrounded by a ring of three density peaks (marked 'x'). Six regions of lower density, marked 'y' and 'z', in turn encircle this central arrangement.

## DISCUSSION

Here we present the first structural view of a member of the Amt family. CryoEM and AFM of 2D crystals showed particles with three-fold symmetry when viewed perpendicular to the membrane plane. The two crystallographically independent views indicate that the most likely molecular envelope is as shown in Fig 4A. AmtB thus seems to form a trimeric structure, consistent with the trimeric nature of the purified protein observed by analytical ultracentrifugation (Blakey *et al*, 2002). Each particle of projected density occupies an area of approximately 4,900 Å<sup>2</sup>, which is entirely consistent with a single trimer of AmtB containing 33

TMH (Thomas *et al*, 2000; von Wirén & Merrick, 2004), assuming an average projected area of approximately  $140 \text{ \AA}^2$  per TMH (Veenhoff *et al*, 2002).

Determination of the oligomeric state of membrane proteins is a topic of growing interest, particularly as the structure of the protein in detergent may not always reflect the physiologically relevant state (Veenhoff *et al*, 2002). However, in this case, the unusually stable state of AmtB in SDS allowed us to confirm that the protein is a trimer in the membrane of wild-type *E. coli* cells. Consequently, we can be reasonably confident that the trimeric crystal structure reported here reflects not only the structure of the purified protein in solution but also the native state of the protein.

With our data limited to  $12 \text{ \AA}$  resolution, the EM projection maps fit both  $p3$  and  $p321$  symmetry. The apparent  $p321$  symmetry could arise through one of two routes: either the crystal is composed of two oppositely oriented layers of protein related by an in-plane intermolecular two-fold axis, or there exists an intramolecular pseudo-two-fold symmetry indistinguishable from a crystallographic two-fold at the current resolution. AFM measurements of the thickness of most crystalline sheets are consistent with the notion of a double layer, but the surface topography of the single layers seems similar to that of the double layers, albeit more disordered. If so, both layers are oriented in the same way and therefore not related by a two-fold symmetry. On the other hand, an intramolecular pseudo-two-fold axis in the crystal plane could also be caused by an internal homology between N- and C-terminal halves of the protein (Dutzler *et al*, 2002; Murakami *et al*, 2002; Van den Berg *et al*, 2004). However, multiple alignments of over 100 Amt sequences showed no obvious evidence of such internal homology in this family at the sequence level (M. Merrick, unpublished). It is interesting to note that AFM images, showing only the surface features of the molecule, rather than projected density, also seem to have an internal two-fold symmetry (Fig 3D). This apparent symmetry can only arise as a pseudo-symmetry manifested at the limited resolution currently attained.

AFM and cryoEM show complementary structural information, namely, surface features and internal structure, respectively. In AFM experiments, it is likely that the cytoplasmic face of the protein, with an overall positive charge, binds to the negatively charged mica substrate. Therefore, the surface features observed are in all probability those of the periplasmic face of AmtB, and the most likely cause of the prominent feature near the three-fold axis is the 31-residue loop between helices II and III (Thomas *et al*, 2000).

AFM showed that double-layered crystals were generally better ordered, as EM images were selected for computer processing on the basis of diffraction quality, it is likely that these were from double layers. The  $12 \text{ \AA}$  projection map of these AmtB crystals (Fig 5B) shows several low-density regions that may represent pores in the protein and several high-density regions that may represent projected  $\alpha$ -helical density. However, given the uncertainty of the nature of the superposition of densities from different crystal layers in the projections of Fig 4, a definite identification of such features is not possible. The one feature that must be coincident in both layers of protein (that is, the centre of each particle at the three-fold axis) is also the lowest density feature within each AmtB particle ('w' in Fig 5B). This is of a comparable density to that of the lipid surrounding the protein,

suggesting that it is not a perpendicular channel running right through the protein, because such a feature would be expected to have considerably lower density (Mindell *et al*, 2001).

Of the known quaternary structures of membrane transport proteins, a trimeric architecture seems comparatively rare. For example, the majority of secondary transporters studied in detail seem to be monomeric, dimeric or tetrameric (Veenhoff *et al*, 2002), and channels of known structure are all dimeric, tetrameric, pentameric or heptameric (Chang *et al*, 1998; Doyle *et al*, 1998; Bass *et al*, 2002; Dutzler *et al*, 2002). We are not aware of any trimeric channels. However, we are aware of structural data for three secondary transporters that are trimeric: the multidrug-proton antiporter, AcrB (Murakami *et al*, 2002); the tetracycline-proton antiporter, TetA (Yin *et al*, 2000); and the sodium-glycine betaine symporter, BetP (Ziegler *et al*, 2004). In the case of AcrB, it is clear that the trimeric assembly is necessary for function, as drugs are transported through a channel formed at the interface of the three subunits. In the case of TetA, it is more likely that, by analogy to other major facilitator superfamily (MFS) proteins, each monomer contains a transport channel (Abramson *et al*, 2003) so that the role of the trimeric architecture in function is less clear. BetP is notable in that the monomers within the trimer seem to have different conformations. We have found no evidence for this type of conformational heterogeneity in AmtB. Both AcrB and members of the MFS, which includes TetA, lactose permease and the glycerol-3-phosphate antiporter, show a pseudo-two-fold symmetry within the monomer. We see evidence for a similar pseudo-symmetry in our projection structures of AmtB.

### Speculation

In bacteria and archaea, *amtB* is invariably linked to the gene *glnK*, and in *E. coli* we have shown that AmtB activity is regulated by interaction with GlnK, which is also a trimer (Coutts *et al*, 2002; Javelle *et al*, 2004) and has a similar footprint to AmtB when viewed down the three-fold axis (Xu *et al*, 1998). It is possible that the trimeric structure of both proteins may reflect a symmetry required for interaction between the two proteins. Whether the trimeric state of AmtB is necessary for function is as yet unknown, but we would speculate that each monomer contains an ammonium channel. Furthermore, as Amt proteins from bacteria, archaea, fungi and plants show a high degree of homology, it is tempting to suggest that this conservation could be reflected in the tertiary and quaternary structures. Fungal and plant Amt proteins and human Rh proteins are thought to be oligomeric (Eyers *et al*, 1994; Marini & Andre, 2000; Ludewig *et al*, 2003) and may also occur as homo- or heterotrimers.

### METHODS

**Crystallization.** C-terminally histidine-tagged AmtB was expressed in *E. coli* and purified as described by Blakey *et al* (2002) with the exception that the construct did not contain a linker between the native sequence and the tag. AmtB was concentrated to  $0.5 \text{ mg ml}^{-1}$  using Amicon Centricon concentrators (molecular weight cut-off 100,000). Purified protein was mixed with DMPC (Avanti Polar Lipids, Alabaster, AL, USA) solubilized in 2% decyl- $\beta$ -D-maltoside to yield LPRs of between 0.4 and  $1.4 \text{ (w/w)}$  at a final protein concentration of  $0.4 \text{ mg ml}^{-1}$  and total volume of  $100 \mu\text{l}$ . The solution was dialysed against  $50 \text{ mM}$  Tris buffer at pH 8.0,  $250 \text{ mM}$  NaCl and 0.005% sodium

azide in a home-built dialysis machine (Jap *et al*, 1992) at 20 °C for 10 days.

**Electron microscopy.** Crystals were embedded in 1% (w/v) glucose. Micrographs were recorded on a Philips CM200 FEG EM. Grids were mounted on an Oxford cold stage and cooled to around -180 °C. Images were recorded at 200 kV at a magnification of about  $\times 50,000$  and a total dose of  $\sim 10 \text{ e}^- \text{ \AA}^{-2}$  on Kodak SO-163 film, developed in concentrated D19 developer for 12 min.

**Image processing.** Micrographs were digitized in steps of 7  $\mu\text{m}$  on a Zeiss SCAI densitometer. Image processing followed procedures described previously (Henderson *et al*, 1986; Crowther *et al*, 1996). Origin and phase CTF refinement were performed with Fourier terms limited to 12  $\text{\AA}$  resolution and symmetry analysis was carried out using ALLSPACE (Valpuesta *et al*, 1994). Amplitudes from individual images were corrected by temperature factors of between 110 and 967  $\text{\AA}^2$  with SCALIMAMP3D (Schertler *et al*, 1993) before averaging. Rotational correlation coefficients were calculated using IMAGIC (van Heel *et al*, 1996).

**Atomic force microscopy.** A stock solution of crystals was diluted tenfold in 20 mM Tris-HCl, 150 mM KCl and 15 mM  $\text{MgCl}_2$  at pH 8.1 (imaging buffer) and adsorbed for > 60 min on freshly cleaved muscovite mica. After adsorption, the sample was gently washed with imaging buffer. AFM experiments were performed using a Nanoscope Multimode microscope equipped with an infrared laser head, fluid cell and oxide-sharpened silicon nitride cantilevers of 100 and 200  $\mu\text{m}$  length, and nominal spring constants of 0.08 and 0.06  $\text{N m}^{-1}$  from Olympus Optical Co. (Tokyo, Japan) and Digital Instruments (Santa Barbara, CA, USA), respectively. Topographs were acquired in contact mode at minimal loading forces ( $\leq 100 \text{ pN}$ ). Trace and retrace signals were recorded simultaneously at line frequencies ranging between 4.1 and 5.5 Hz. Correlation averages were calculated from AFM topographs with the SEMPER image processing system (Saxton, 1996). Perspective views were prepared using the SXM program (University of Liverpool, UK).

**Western blotting and cell fractionation.** These were carried out as described by Coutts *et al* (2002).

**Supplementary information** is available at *EMBO reports* online (<http://www.emboreports.org>).

**Note added in proof.** Since submission of this manuscript, the 3D crystal structure of AmtB has been published by two groups (Khademi *et al* (2004) *Science* **305**: 1587–1594; Zheng *et al* (2004) *Proc Natl Acad Sci USA*, in press). These crystal structures confirm and extend the findings presented here.

#### ACKNOWLEDGEMENTS

We thank Dr P. Wang for excellent microscopy support, Mr J. Thornton for preparation of the AmtB antibody, Dr A. Javelle for Fig 1 and Dr A. Durand for constructive criticism of the manuscript. P.B., M.C., D.B. and M.M. acknowledge generous support from the BBSRC (UK). A.E. acknowledges support by the Swiss National Research Foundation, the ME Müller Foundation, the Swiss National Center of Competence in Research (NCCR) 'Structural Biology' and the NCCR 'Nanoscale Science'.

#### REFERENCES

Abramson J, Smirnova I, Kasho V, Verner G, Kaback HR, Iwata S (2003) Structure and mechanism of the lactose permease of *Escherichia coli*. *Science* **301**: 610–615

Bass RB, Strop P, Barclay M, Rees DC (2002) Crystal structure of *Escherichia coli* MscS, a voltage-modulated and mechanosensitive channel. *Science* **298**: 1582–1587

Blakey D, Leech A, Thomas GH, Coutts G, Findlay K, Merrick M (2002) Purification of the *Escherichia coli* ammonium transporter AmtB reveals a trimeric stoichiometry. *Biochem J* **364**: 527–535

Chang G, Spencer RH, Lee AT, Barclay MT, Rees DC (1998) Structure of the MscL homolog from *Mycobacterium tuberculosis*: a gated mechanosensitive ion channel. *Science* **282**: 2220–2226

Coutts G, Thomas G, Blakey D, Merrick M (2002) Membrane sequestration of the signal transduction protein GlnK by the ammonium transporter AmtB. *EMBO J* **21**: 1–10

Crowther RA, Henderson R, Smith JM (1996) MRC image processing programs. *J Struct Biol* **116**: 9–16

Doyle DA, Morais Cabral J, Pfuetzner RA, Kuo A, Gulbis JM, Cohen SL, Chait BT, MacKinnon R (1998) The structure of the potassium channel: molecular basis of  $\text{K}^+$  conduction and selectivity. *Science* **280**: 69–77

Dutzler R, Campbell EB, Cadene M, Chait BT, MacKinnon R (2002) X-ray structure of a ClC chloride channel at 3.0  $\text{\AA}$  reveals the molecular basis of anion selectivity. *Nature* **415**: 287–294

Eyers SA, Ridgwell K, Mawby WJ, Tanner MJ (1994) Topology and organization of human Rh (rhesus) blood group-related polypeptides. *J Biol Chem* **269**: 6417–6423

Henderson R, Baldwin JM, Downing KH, Lepault J, Zemlin F (1986) Structure of purple membrane from *Halobacterium halobium*—recording, measurement and evaluation of electron-micrographs at 3.5  $\text{\AA}$  resolution. *Ultramicroscopy* **19**: 147–178

Jap BK, Zulauf M, Scheybani T, Hefti A, Baumeister W, Aebi U, Engel A (1992) 2D crystallization: from art to science. *Ultramicroscopy* **46**: 45–84

Javelle A, Severi E, Thornton J, Merrick M (2004) Ammonium sensing in *E. coli*: the role of the ammonium transporter AmtB and AmtB-GlnK complex formation. *J Biol Chem* **279**: 8530–8538

Ludewig U *et al* (2003) Homo- and hetero-oligomerization of AMT1  $\text{NH}_4^+$ -uniporters. *J Biol Chem* **278**: 45603–45610

Marini A-M, Andre B (2000) *In vivo* N-glycosylation of the Mep2 high-affinity ammonium transporter of *Saccharomyces cerevisiae* reveals an extracytosolic N-terminus. *Mol Microbiol* **38**: 552–564

Marini A-M, Matassi G, Raynal V, Andre B, Cartron J, Cherif-Zahar B (2000) The human Rhesus-associated RhAG protein and a kidney homologue promote ammonium transport in yeast. *Nat Genet* **26**: 341–344

Mindell JA, Maduke M, Miller C, Grigorieff N (2001) Projection structure of a ClC-type chloride channel at 6.5  $\text{\AA}$  resolution. *Nature* **409**: 219–223

Monahan BJ, Unkles SE, Tsing IT, Kinghorn JR, Hynes MJ, Davis MA (2002) Mutation and functional analysis of the *Aspergillus nidulans* ammonium permease MeaA and evidence for interaction with itself and MepA. *Fungal Genet Biol* **36**: 35–46

Murakami S, Nakashima R, Yamashita E, Yamaguchi A (2002) Crystal structure of bacterial multidrug efflux transporter AcrB. *Nature* **419**: 587–593

Quentin F, Eladari D, Cheval L, Lopez C, Goossens D, Colin Y, Cartron JP, Paillard M, Chambrey R (2003) RhBG and RhCG, the putative ammonia transporters, are expressed in the same cells in the distal nephron. *J Am Soc Nephrol* **14**: 545–554

Saxton WO (1996) SEMPER: distortion compensation, selective averaging, 3-D reconstruction, and transfer function correction in a highly programmable system. *J Struct Biol* **116**: 230–236

Schertler GF, Villa C, Henderson R (1993) Projection structure of rhodopsin. *Nature* **362**: 770–772

Thomas GH, Mullins JG, Merrick M (2000) Membrane topology of the Mep/ Amt family of ammonium transporters. *Mol Microbiol* **37**: 331–344

Valpuesta JM, Carrascosa JL, Henderson R (1994) Analysis of electron microscope images and electron diffraction patterns of thin crystals of phi 29 connectors in ice. *J Mol Biol* **240**: 281–287

Van den Berg B, Clemons WMJ, Collinson I, Modis Y, Hartmann E, Harrison SC, Rapoport TA (2004) X-ray structure of a protein-conducting channel. *Nature* **427**: 36–44

van Heel M, Harauz G, Orlova EV (1996) A new generation of the IMAGIC image processing system. *J Struct Biol* **116**: 17–24

Veenhoff LM, Heuberger EHML, Poolman B (2002) Quaternary structure and function of transport proteins. *Trends Biochem Sci* **27**: 242–249

von Wirén N, Merrick M (2004) Regulation and function of ammonium carriers in bacteria, fungi and plants. *Top Curr Genet* **9**: 95–120

- von Wirén N, Lauter FR, Ninnemann O, Gillissen B, Walch-Liu P, Engels C, Jost W, Frommer WB (2000) Differential regulation of three functional ammonium transporter genes by nitrogen in root hairs and by light in leaves of tomato. *Plant J* **21**: 167–175
- Westhoff CM, Ferreri-Jacobia M, Mak DO, Foscett JK (2002) Identification of the erythrocyte Rh-blood group glycoprotein as a mammalian ammonium transporter. *J Biol Chem* **277**: 12499–12502
- Xu Y, Cheah E, Carr PD, van Heeswijk WC, Westerhoff HV, Vasudevan SG, Ollis DL (1998) GlnK, a PII-homologue: structure reveals ATP binding site and indicates how the T-loops may be involved in molecular recognition. *J Mol Biol* **282**: 149–165
- Yin CC, Aldema-Ramos ML, Borges-Walmsley MI, Taylor RW, Walmsley AR, Levy SB, Bullough PA (2000) The quaternary molecular architecture of TetA, a secondary tetracycline transporter from *Escherichia coli*. *Mol Microbiol* **38**: 482–492
- Ziegler C, Morbach S, Schiller D, Kramer R, Tziatzios C, Schubert D, Kuhlbrandt W (2004) Projection structure and oligomeric state of the osmoregulated sodium/glycine betaine symporter BetP of *Corynebacterium glutamicum*. *J Mol Biol* **337**: 1137–1147